Decomposition of fMRI into Multiple Components

François G. Meyer
Department of Electrical Engineering, University of Colorado at Boulder
Department of Radiology, University of Colorado Health Sciences Center
E-mail: francois.meyer@colorado.edu.

ABSTRACT

The goal of this work is to provide a new representation of functional magnetic resonance imaging (fMRI) time series. Functional neuroimaging aims at quantifying and localizing neuronal activity using imaging techniques. Functional MRI can detect and quantify hemodynamic changes induced by brain activation and neuronal activity. The time course of the fMRI signal at a given voxel inside the brain is represented with a structural model where each component of the model belongs to a subspace spanned by a small number of basis functions. The basis functions in different subspaces have very distinct time-frequency characteristics. The large scale trend of the signal is represented with a combination of large scale wavelets. The response to the stimulus is expanded on a small set of basis functions. Because it is critical to adapt the basis functions to the type of stimulus, the evoked response to a random presentation is expanded into small scale wavelets or wavelet packets, while the response to a periodic stimulus is represented with cosine or sine functions. We illustrate the estimation of the components of the model with several experiments.

1. INTRODUCTION

Functional brain imaging utilizes the coupling between local electrical activity and regional changes in blood flow and blood oxygenation level. Functional MRI can estimate regional changes in cerebral blood flow and blood oxygenation level. Blood Oxygenation Level-Dependent (BOLD) fMRI uses deoxyhemoglobin as contrast agent : deoxygenated hemoglobin induces a difference in magnetic susceptibility relative to the surrounding. This local modification of the susceptibility can be measured, and maps of changes in cerebral venous oxygen concentration can be obtained. The cascade of physiological events that trigger the changes in the BOLD signals remains an area of active research.[1] One interpretation of the BOLD effect is provided by the following scenario. The local electrical activity induced by the firing of the neurons increases the consumption of oxygen and glucose. About 100 *ms* after the onset of cortical activity, this regional demand in oxygen results in an increase in deoxyhemoglobin concentration. This increase in deoxyhemoglobin, which is well localized around the area of electrical activation,[1] corresponds to the initial dip of the BOLD signal. About 500 *ms* later, a regulatory mechanism causes capillary vessels to dilate, and blood flow to increase. At about 1s after the onset of electrical activity, deoxyhemoglobin decreases as oxygenated blood arrives in the capillaries. The oxygen supply becomes much larger than the demand, and the relative excess in oxyhemoglobin can be measured by the BOLD technique.

Unfortunately, changes in the fMRI signal occurring during brain activation are very small: 1-5%. This detection is further complicated by the presence of a large number of instrumental and physiological noises that contaminate the fMRI signal. These contaminants should be estimated and removed in order to avoid a loss of sensitivity in the detection of the stimulus induced response. A first source of artifacts includes physiological noise due to cardiac and respiratory functions. Respiration induces magnetic field susceptibility changes in the lungs, which induce magnetic field shifts in the brain.[2] Artifacts related to the cardiac function have several origins: (i) pulsatile bulk motion of the vessels, (ii) flow artifacts, (iii) and long term drift of the oxygen saturation level due to breathing depth autoregulation.[2] Cardiac pulsations of the brain also induce CSF flow ; because the CSF has a very long T1, this can be the source of artifacts occurring at the cardiac frequency. A second source of artifacts consists in non periodic noise with a $1/f$ spectrum due to long term physiological drifts, and instrumental instability. These highly nonlinear trends can vary across neighboring voxels. Finally, there is also some white noise caused by thermal and quantum noise. Other effects include head motion, motion of the eyes, and resting brain fluctuations caused by spontaneous fluctuation in regional cerebral blood flow. These effects will not be discussed here. One can

This work was supported by a Whitaker Foundation Biomedical Engineering Research Grant.

assume that head motion has been compensated, and one will ignore resting brain fluctuations. While a number of standard statistical signal processing techniques are currently being used to estimate and remove some of the components,[3] we propose to directly model the time series at any given voxel in the brain with a structural model. Each component of this model has a meaningful physiological interpretation. In order to keep the number of parameters of the model as small as possible, each component of the model belongs to a subspace spanned by a small number of basis functions. The basis functions in different subspaces have very distinct time-frequency characteristics. The large scale trend of the signal is represented with a combination of large scale wavelets. The response to the stimulus is also expanded on a small set of basis functions. Because it is critical to adapt the basis functions to the type of stimulus, the evoked response to a random presentation is expanded into small scale wavelets or wavelet packets, while the response to a periodic stimulus is represented with cosine or sine functions. The next section presents some of the sources of noise and signal variation in the fMRI signal. Section 2.2 describes the structural model for the fMRI signal. The identification and estimation of the model is presented in section 3. Finally, results of experiments conducted on fMRI data are presented in section 4.

2. STRUCTURAL MODEL OF THE *F*MRI TIME SERIES

2.1. What is inside the fMRI signal ?

In general the fMRI time series at a given voxel in the brain is a complicated mixture of signals. We examine here the main components of the fMRI signal, and their time-frequency characteristics. We choose to represent the BOLD signal as the sum or three components:

$$s(t) = \theta(t) + a(t) + n(t) \tag{1}$$

where :

- $\theta(t)$ is a trend, or baseline drift. This drift is a slowly varying signal, due to long term physiological drifts, and instrumental instability. The drift, mostly composed of low frequencies, can also include the aliased cardiopulmonary physiological noise .
- $a(t)$ is a signal induced by neuronal activation. This signal will only exist if the voxel is inside a functionally activated brain area.
- $n(t)$: a white noise caused by thermal and quantum noise

2.1.1. Baseline drift: $\theta(t)$

The fMRI signal often exhibits a trend: the signal increases or decreases steadily over time. This long term variability can be extremely different from one voxel to another (even for neighboring voxels, as shown in Fig. 1). This global trend can be observed under the baseline condition, and is not a consequence of the stimulus. If the trend is not removed, any analysis based on correlation methods will be tracking the large scale variation in the signal, instead of the effects of the stimulus. Baseline drifts have been described by linear,[3] and polynomial[4] functions of time. As shown in the experiments (section 4) the trend fluctuates slowly, and splines, or large scale wavelets describe the large scale variations of the signal over time better than a straight line.

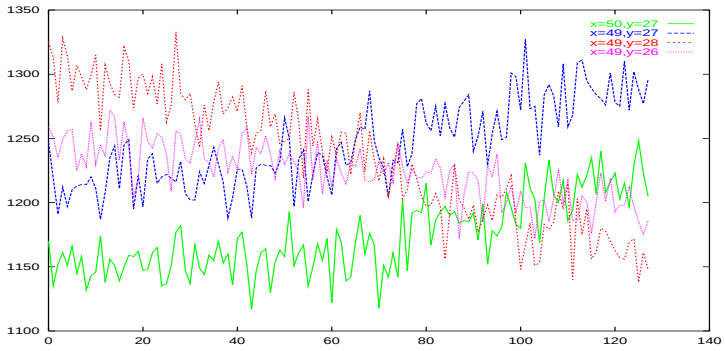

Figure 1. Time course of four neighboring voxels. Notice that the drift is going in different directions

2.1.2. Cardio-pulmonary effects

Cardiac (and pulmonary) effects are periodic functions of time, and one could in principle design a notch filter that would cancel out any contribution to the fMRI signal at the cardiac and respiratory frequencies.[5] Unfortunately, the problem is further complicated by the aliasing of the cardiac effects. Because the MR image acquisition rate is usually well below the critical sampling rate required by the cardiac frequency, cardiac effects will be aliased at low frequency. With the knowledge of the cardiac cycle it is possible to estimate the frequency of the aliased signal. In order to estimate the cardiac cycle, the authors in[5] have proposed to measure directly the oxygen saturation level, as well as the respiratory cycle. These time series can then be used to estimate the fundamental frequency of the cardiac and respiratory cycles. Unfortunately, oxygenation level is rarely monitored during fMRI acquisition.

2.1.3. Response to the stimulus : $a(t)$

The exact understanding of the cascade of physiological events that can explain the spatio-temporal characteristics of the BOLD response is still being explored.[6] Optical imaging has provided rich information about the coupling between neural activity and oxygen saturation. The time course of oxygen concentration in the micro-vascular system can be directly measured with optical imaging.[1] It appears that after the onset of stimulation the oxygen concentration rapidly drops in response to the local energy metabolism triggered by the stimulation. The dip is followed by a large hyperoxygenation. The imbalance between oxygen metabolism and oxygen supply is at the origin of the BOLD signal. Several authors have proposed to reduce this complex sequence of effects to a simple linear convolution model:

$$s(t) = (h * x)(t) \tag{2}$$

where $s(t)$ is the fMRI signal, $x(t)$ is the known stimulus waveform (it need not be periodic), and $h(t)$ is the unknown hemodynamic response function that not only characterizes the complex interaction between the hemodynamic response and the stimulus, but also takes into account the image acquisition process. This linear model is appealing because it allows to exploit the standard machinery of linear models in the time domain, or the standard signal processing machinery in the Fourier domain. Lange and Zeger[7] use a parametric gamma model, and allow $h(t)$ to vary from one part of the brain to another. Again, their approach is limited to periodic stimuli. Crellin et al[8] proposed a semi-parametric approach where $h(t)$ is estimated using spline basis functions. The major and profound limitation of the model (2) is the assumption of linearity. Indeed it has become clear that there is a nonlinear relationship between the variation in the fMRI signal and the stimulus presentation.[9,4] Consequently the linear model in equation (2) will fail to represent accurately the nonlinear structure present in the fMRI data.

2.2. Structural model of the fMRI time series

As explained above the fMRI signal can be decomposed as the sum of three main effects: a baseline drift, (which may include cardio-pulmonary effects), a response to the stimulus, and some uncorrelated noise. In principle it could be possible to represent each component with a parametric model. However, in the absence of any detailed substantive understanding of the mechanism of the fMRI response, we believe that a non parametric data-driven approach, which does not require knowledge of some predefined explanatory basis functions, will better account for all important features present in the components. A fully exploratory analysis of the raw fMRI data can be performed, and should reveal in principle the main features of the data. Formally, we could try to estimate a set of basis elements Φ_{λ_i}, and a set of coefficients α_i, depending on some frequency, or scale, parameter λ_i such that the observed data $s(t)$ can be described by:

$$s(t) = \sum_i \alpha_i \Phi_{\lambda_i}(t) + n(t) \tag{3}$$

where $n(t)$ is some thermal white acquisition noise. In this model each coordinate α_i corresponds to a different component Φ_{λ_i} of the fMRI signal; one of this component is assumed to be the response to the stimulus, while others are physiological and technological confounds. A stochastic formulation would give rise to the following representation:

$$s(t,\omega) = \sum_i \alpha_i(\omega) \Phi_{\lambda_i}(t) + n(t,\omega) \tag{4}$$

where $s(t,\omega)$ is a stochastic process and the coefficients $\alpha_i(\omega)$ are independent random variables. If one assumes that the α_i are Gaussian, then (4) is the principal component analysis problem.[10,11] If the coefficients are non Gaussian, then the problem (4) is known as the independent component analysis problem.[12–14] There has been

no evidence that the fMRI data are Gaussian, and therefore the principal component analysis cannot be justified. While ICA can handle non Gaussian signals, the technique also suffers from a number of shortcomings.[15] A more fundamental problem associated with this approach is the interpretation of the Φ_{λ_i} in terms of meaningful components. The interpretation of the Φ_{λ_i} usually rely on ad hoc heuristics such as visual inspection of the similarity between the Φ_{λ_i} and the stimulus time series. Clearly, this approach is not suited to even-related stimuli, or graded temporal response. Alternatively, instead of letting the data "speak for themselves" one can choose to project the fMRI signal on some carefully chosen basis functions. Examples of such basis functions are splines, cosine / sine functions, or wavelets. Smoothly varying signals can be efficiently described using splines, and the author in[8] have tried to estimate the fMRI signal with such techniques. Another approach consists in representing the signal with a Fourier basis. The Fourier basis is efficient when there is a reason to believe that the signal is stationary, i.e. when the local statistical properties are invariant in time. In our problem, the hemodynamic response to periodic stimuli can probably be considered as stationary (after having removed any signal drift), and Fourier bases have been used somewhat successfully in this context.[7,16] However, event induced hemodynamic responses are not stationary: they contain transients, global drifts, etc.

In order to represent efficiently the different components of the fMRI signal, one needs enough flexibility to adapt the representation to the time-frequency properties of each component. If one accepts to give up the requirement that the Φ_{λ_i} form an orthogonal basis, then it becomes possible to describe each component with a small set of basis functions taken from several different libraries of basis functions. Since the goal of fMRI is the detection of the stimulus response, the detection problem would be greatly facilitated if one could find a coordinate system within which the confounds, and the stimulus response correspond to independent subspaces. Calculating the stimulus induced response would then simply consist in projecting the observation onto the "response subspace". In this work, we propose to represent the fMRI signal with a structural model where each component of the model has a direct interpretation, and is able to pick up some of the salient characteristics of the data.

1. A small set of large scale wavelets $\varphi_j(t)$ describe the smooth slowly varying baseline drift:

$$\theta(t) = \sum_{j=0}^{J-1} a_j \varphi_j(t) \tag{5}$$

   Wavelets with many vanishing moments yield very sparse decompositions of piece-wise smooth signals ; therefore they provide a very appropriate tool to approximate the low frequency trends occurring at a large scale in the signal.[17]

2. A small number of small scale wavelets, or wavelet packets, $\psi_i(t)$ represent the transient induced by an event-related stimulus:

$$a(t) = \sum_{i=0}^{I-1} d_i \psi_i(t) \tag{6}$$

   Wavelet packets are "time frequency atoms" that can be constructed using wavelet filters. Wavelets and wavelet packets can efficiently describe the local behavior of a signal, by "zooming in" on the singularities, or transients. Wavelet packets have been used to characterize transients in electroencephalograms.[18,19]

3. A small number of cosine functions $\omega_k(t)$ represent the response to a periodic stimulus:

$$a(t) = \sum_{k=0}^{K-1} c_k \omega_k(t) \tag{7}$$

   Assuming that a periodic stimulus induces a periodic response, then a cosine (or a Fourier basis) is the ideal representation for representing such a signal.

Each set of wavelets, wavelet packets, and Fourier basis functions is optimal to represent the corresponding component. Consequently, the coefficients of such a decomposition are meaningful, and provide rich information about

the data being analyzed. To summarize the fMRI signal can be written as:

$$s(t) = \begin{cases} \sum_{j=0}^{J-1} a_j \varphi_j(t) + \sum_{i=0}^{I-1} d_i \psi_i(t) & \text{for an event-related stimulus} \\ \text{or} & \\ \sum_{j=0}^{J-1} a_j \varphi_j(t) + \sum_{k=0}^{K-1} c_k \omega_k(t) & \text{for a periodic stimulus} \end{cases} \tag{8}$$

3. IDENTIFICATION AND ESTIMATION OF THE MODEL

The fMRI signal in (8) is now represented by a linear combination of functions that do not form an orthonormal basis: wavelets for instance are not designed to be orthogonal to cosine, or sine functions. As is obvious from equations (8), there are now many possible choices for the coefficients a_j, d_i, c_k, and the corresponding I, J, K. Because our analysis requires an unambiguous interpretation of the coefficients, we choose to analyze the time course $s(t)$ with a fixed collection of basis functions that are selected from two libraries of basis functions. This construction allows in principle to obtain a unique decomposition by using oblique projections as explained in.[20] We present here the algorithm for the decomposition of $s(t)$. A different analysis is performed for periodic, and non periodic stimulus response. The analysis of sudden evoked response is first described.

3.1. Representation of the response to a non periodic event-related stimulus

The raw fMRI signal is first expanded into a wavelet basis:

$$s(t) = \Phi_{J_0}(t) + \sum_{j=0}^{J_0} \sum_{k=0}^{2^{J-j}} \psi_{j,k} \tag{9}$$

where j is the scale index, and k is the translation index. The decomposition is performed up to the coarsest scale $J_0 = \log(N)$, where N is the size of the time series $s(t)$. The trend $\theta(t)$ is defined as the coarse scale part of $s(t)$ in (9):

$$\theta(t) = \Phi_{J_0}(t) + \sum_{j=J_0-J+1}^{J_0} \sum_{k=0}^{2^{J-j}} \psi_{j,k} \tag{10}$$

After removing the trend, the signal $a(t) + n(t)$ is projected on a wavelet packet basis in order to separate the noise $n(t)$ from the signal $a(t)$. Because the stimulus and the trend have very different time-frequency characteristics one should switch to another basis to separate $a(t)$ from $n(t)$. By definition, the signal $a(t) + n(t)$ lives in the space orthogonal to the large scale wavelets that constitute the trend: $[\text{span}\{\phi_j, j = J, .., J_0\}]^{\perp}$. A basis of that space can be constructed from wavelet packets.

3.1.1. Best denoising wavelet packet basis

It is possible to use a divide and conquer algorithm to select the best wavelet packets basis of the space $[\text{span}\{\phi_j, j = J, .., J_0\}]^{\perp}$. After excluding the nodes corresponding to the large scale wavelets : $\{\phi_j; j = J, .., J_0\}$ (see Fig. 2), a standard best basis search can be performed on all the remaining dyadic nodes. The criterion for the best basis search is the optimal reconstruction of $a(t)$ from $a(t) + n(t)$. Let $\hat{a}(t)$ be the signal reconstructed after thresholding the wavelet packet coefficients $< a + n, \psi_i >$ of $a(t) + n(t)$. Then the approximation error is given by:

$$\|a(t) - \hat{a}(t)\|^2 \tag{11}$$

Krim[21] proposed the following estimator for the approximation error:

$$e(\{< a + n, \psi_i >\}) = \sum_{i=0}^{N-1} \mathcal{T}(| < a + n, \psi_i > |) \tag{12}$$

with

$$\mathcal{T}(u) = \begin{cases} u - \sigma^2 & \text{if} \quad u \leq T^2 \\ \sigma^2 & \text{if} \quad u > T^2 \end{cases} \tag{13}$$

where σ is the variance of $n(t)$, and T is a threshold. The function $e(\{< a+n, \psi_i >\})$ defines the cost function that is optimized during the search of the best basis. After the best basis is selected, the signal is reconstructed using the hard thresholding strategy defined by $\mathcal{T}(u)$ in (13).

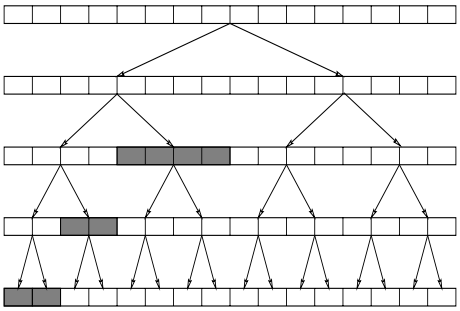

Figure 2. The trend is composed of low scale wavelets coefficients (shaded boxes). A wavelet packet basis is built using all other boxes that lie on a dyadic grid.

3.2. Representation of the response to a periodic stimulus

As in the case of the non periodic stimulus, the raw fMRI signal is first expanded into a wavelet basis:

$$s(t) = \Phi_{J_0}(t) + \sum_{j=J_0-J+1}^{J_0} \sum_{k=0}^{2^{J-j}} \psi_{j,k} \tag{14}$$

where j is the scale index, and k is the translation index. The decomposition is performed up to the coarsest scale $J = \log(N)$. The trend $\theta(t)$ is defined as the coarse scale part of $s(t)$ in (14):

$$\theta(t) = \Phi_{J_0}(t) + \sum_{j=J_0-J+1}^{J_0} \sum_{k=0}^{2^{J-j}} \psi_{j,k} \tag{15}$$

The scaling function $\Phi_{J_0}(t)$, and the wavelets $\psi_{j,k}, j = J - J_0 + 1, \ldots, J; k = 0 \ldots 2^{J-j}$ constitute the first J_0 elements of the basis.

If the stimulus is periodic, clearly a Fourier – or a cosine – basis should be used. Any combination of wavelets and cosine functions do not in general result in a basis : the wavelets and the cosines are usually not independent. The construction of a basis is still possible if the cosine that are highly correlated to the large scale wavelets are removed. The cosine functions ω_k with the smallest frequency $k = 0, \ldots, J-1$ are removed, and the detrended signal is projected onto the set $\{\omega_k,\ k = J, \ldots, J_0\}$. As above the coefficients are thresholded using a hard thresholding rule similar to (13). A signal $\hat{a}$ is then reconstructed from the thresholded coefficients. A more rigorous analysis involves the construction of a basis, and oblique projections of the signal onto the two subspaces spanned by the wavelets on one hand, and the cosine functions on the other. This construction is detailed in.[20]

4. EXPERIMENTS

4.1. Response to an event-related stimulus

We illustrate here the principle of the algorithm with some data provided by Gregory McCarthy (Brain Imaging and Analysis Center, Duke University), that demonstrate prefrontal cortex activation in the presence of infrequent events.[22] Visual stimuli were presented to the subjects : most of the images were squares. Infrequent events consisted in the appearance of circles at time 11, 43, 53, 64, 73, 97, and 111. Occasionally, images of everyday objects were also presented (at time 24, 33, 88). A picture was displayed every 1.5 seconds. Images were acquired every

1.5 seconds. Each run consisted of 128 images. The subject was asked to mentally count the number of occurrences of the circles, and report that number at the end of the run. Fig. 3-right shows the time series $s(t)$ of a voxel located in the prefrontal cortex. The onset of infrequent events (circles, and everyday objects) are shown with vertical bars. The voxel from where the time series was extracted is pointed at by the arrow in Fig. 3-left. Observe the significant temporal drift in $s(t)$ in Fig. 3-right. The first step of the algorithm is the drift removal. Figure 4-left shows the drift $\theta(t)$ superimposed on the original time-series. Note that an approximation of the drift with a linear trend would not be inaccurate. A wavelet approximation, allows for a smooth nonlinear drift. Once the drift is estimated, one removes its structure and one calculates the remainder $s(t) - \theta(t) = a(t) + n(t)$. Fig. 4-right shows the residual $a(t) + n(t)$. Observe how the resulting time series is well centered around 0. Finally, one seeks the best wavelet packet basis that could separate the signal induced by activation, $a(t)$, from the noise $n(t)$. At this point we have removed the contaminants from the fMRI signal. The final remainder should include only an activation-induced response $a(t)$, if the corresponding voxel is being activated. This signal is shown in Fig. 5. We observe a significant variation of the signal $a(t)$ after the onset of the visual stimuli, delayed by 5 to 6 images. We are currently working on a technique that will allow us to detect significant changes in $a(t)$ directly from the wavelet packet coefficients.

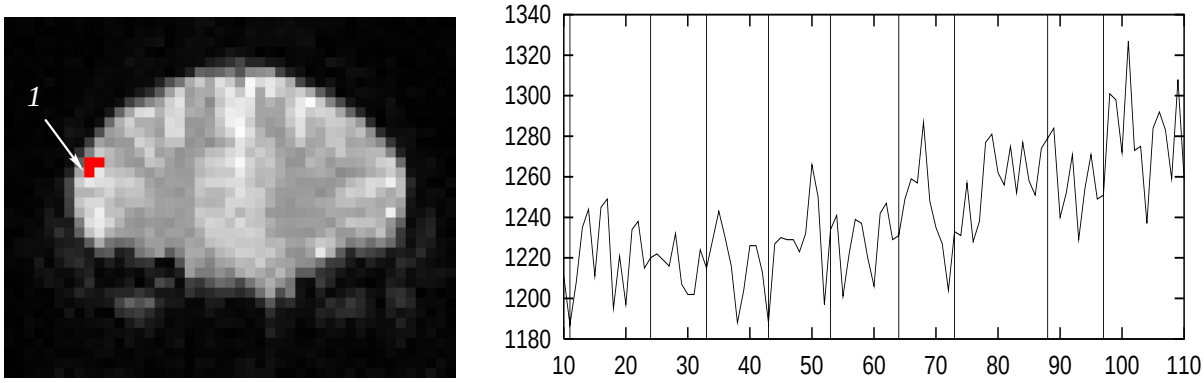

Figure 3. Left: coronal echoplanar image. Right: time course $s(t)$ of one individual voxel pointed at by an arrow. Vertical lines indicate the occurrence of stimuli (see text).

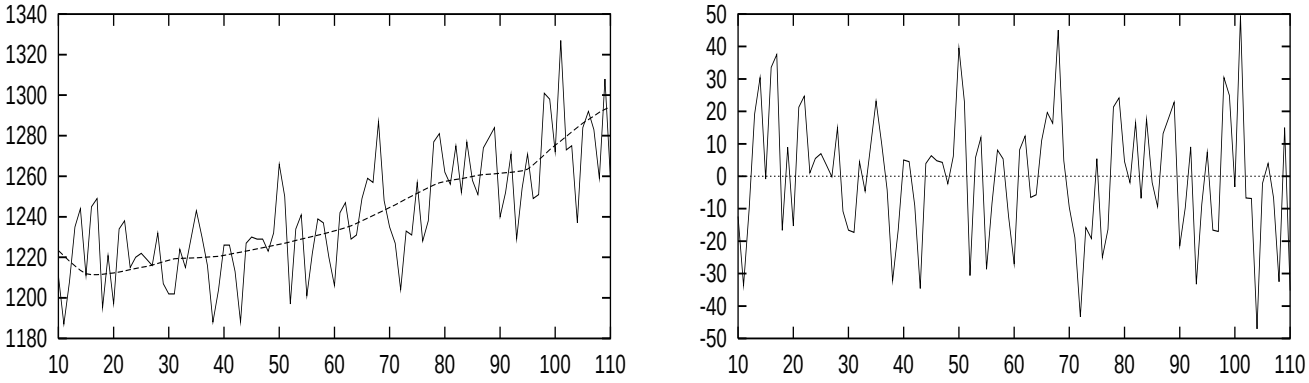

Figure 4. Left: original time series $s(t)$ with the drift superimposed. Right: residual $a(t) + n(t)$ after the drift has been removed.

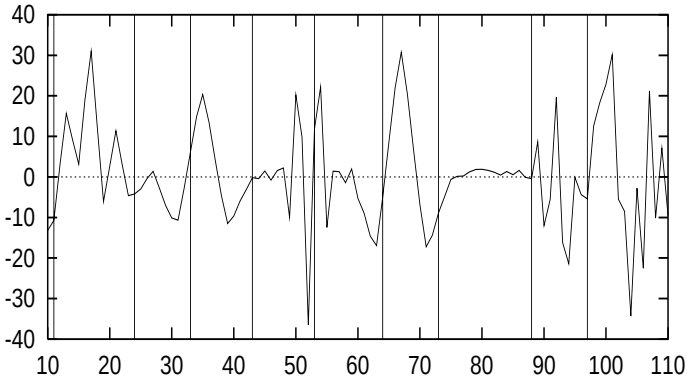

Figure 5. Approximation to the stimulus response $a(t)$ using wavelet packets

4.2. Response to periodic stimulus

We illustrate here the principle of the algorithm with some data provided by Gregory McCarthy, (Brain Imaging and Analysis Center, Duke University), that demonstrate left posterior temporal lobe activation during auditory comprehension.[23] The study involved several subjects who listened passively to alternating sentences spoken in English (their native language), and Turkish (which they did not understand). Each time series was composed of 28 alternating auditory segments of English and Turkish. Each segment lasted for 6 seconds, and images were acquired every 1.5 s. There is a delay of 12 seconds from the first image to the onset of the first sentence. Images were acquired with a 1.5 T General Electric Signa scanner equipped with an ANMR echoplanar system. The subject's head was immobilized using a vacuum cushion and a forehead strap. Functional images were acquired using a gradient-echo echoplanar sequence (TR=1,500, TE=45, $\alpha = 60^o$, NEX=1, FOV=40 $\times$ 20 cm, slice thickness=9mm, skip = 2mm, imaging matrix= 128$\times$ 64, voxel size = 3.2 $\times$ 3.2 $\times$ 9 mm). The images for each of the seven slices were acquired in equally spaced time intervals over the 1.5 second TR in the slice order 1-3-5-7-2-4-6. More details about the experiments are available in.[23]

Figure 9 shows the first image of the first run located in slice 4. A time series was extracted from the voxel (79,39) pointed by the arrow 2 in slice 4, and is displayed in Fig. 6-left. A discrete Fourier transform was computed (the signal was multiplied by a Gaussian window in order to enforce periodicity). The square of the Fourier coefficients are shown in Fig. 6-right. As is obvious from Fig. 6-right most of the energy lies at the low frequencies (note the logarithmic scale).

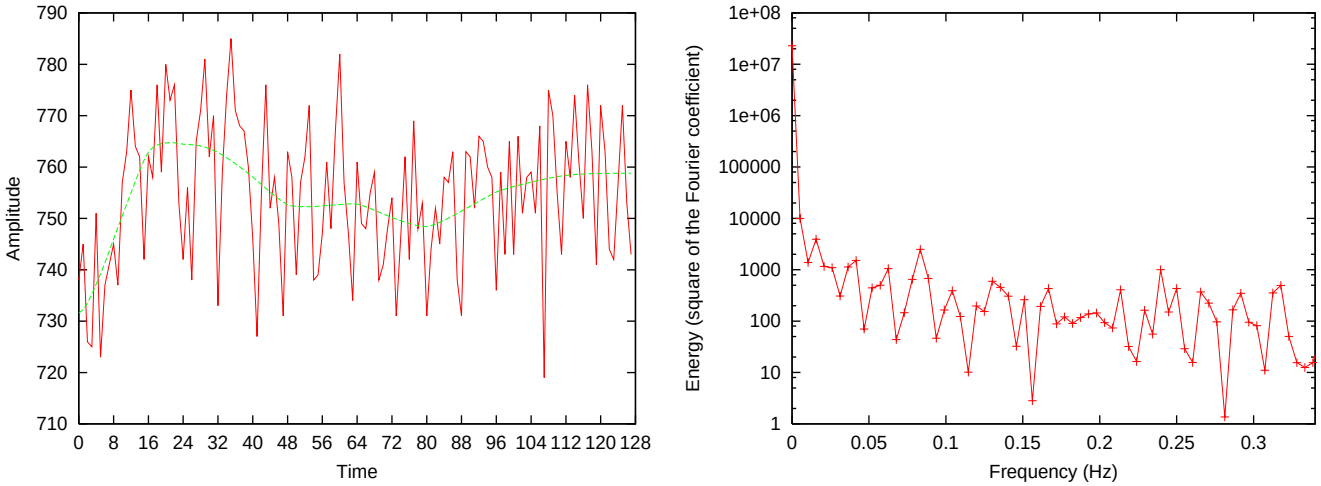

Figure 6. Left: time series $s(t)$, with drift superimposed. Right: Power spectrum of the raw time-series. Most of the energy is located in the low frequency.

The trend $\theta(t)$, defined by (15) is computed. Here we have $J_0 = 7$, and we use $J = 5$. Figure 6-left shows the drift superimposed onto the raw time series. Finally, Fig. 7-left shows the detrended time series, and Fig. 7-right shows the spectrum of the detrended time series. The low frequencies have been removed, one can clearly detect the peak at the frequency of the stimulus (1/12 Hz). A map of the squared Fourier coefficients at the frequency of the stimulus can be generated after detrending. Thresholding this map at a level of 1450 results in the activation map shown in Fig. 8. This map clearly shows activation in the left posterior temporal lobe, and in the left inferior frontal lobe.

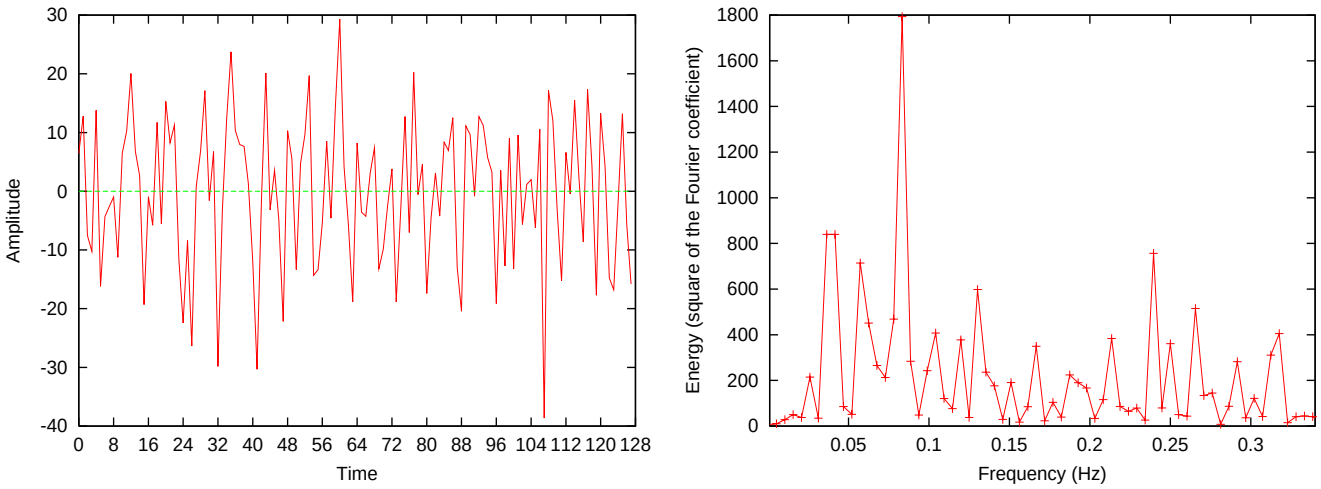

Figure 7. Left: detrended time-series. Right; power spectrum of the detrended time-series

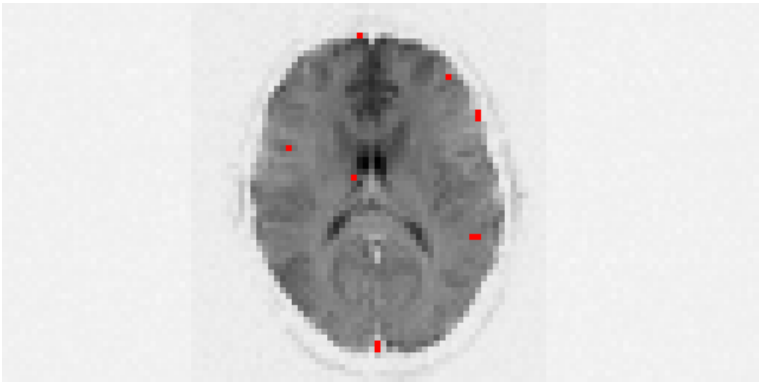

Figure 8. Activation map obtained by thresholding the spectral energy map at the frequency of the stimulus

4.3. Analysis of the detrending performance

We have compared the performance of the detrending algorithm for several values of the scale J of the trend $\theta(t)$. The same value of J was used for all pixels. We analyzed the performance of the detrending using the periodic English-Turkish dataset described in the previous section. A Student t-test was designed to compare the signal under the two conditions: English sentences, or Turkish sentences. Pixels with a P-value less than 0.0005 were deemed activated, and colored in red in the activation maps.

Figure 9 shows an activation map superimposed on the raw EPI data. The map was generated with one run of alternating Turkish/English intervals, starting with Turkish. The map clearly shows activated pixels in the left inferior frontal lobe (region 1), as well as in the left posterior temporal lobe (region 2). Table 1 shows the P-value at the pixels 1 and 2 (pointed at by the arrows in Fig. 9), for several values of J. Detrending clearly decreased the P-value, and as a result increased the size of the activated regions.

Figure 10 shows another activation map superimposed on the raw EPI data. The map was generated with one run of alternating English / Turkish intervals, starting with English. Again, the map shows in red activated pixels in the left inferior frontal lobe (region 1), as well as in the left posterior temporal lobe (region 2). A quantitative analysis of the detrending performance is shown in Table 2 where the *P*-value at the pixels 1 and 2 (pointed at by the arrows in Fig. 9), are displayed for several values of J. Detrending significantly reduced the *P*-value for both pixels 1 and 2. While $J = 4$ even further reduces the *P*-value at pixel 1, the *P*-value increased at pixel 2 for this value of J. One possible explanation is that for $J = 4$, the trend starts tracking the variations in the BOLD signal that are due to the stimulus response. Figure 11 shows the time-series at pixel 1 with the trend superimposed, for several values of J. While the trend estimated for $J = 7, 6$ fail to track the long term variability of the signal, the trend obtained with $J = 4$ (lower left corner) appears to follow too closely the BOLD signal changes. This could explain the loss in sensitivity in region 2. We note that a linear trend (such as the one obtained for $J = 7$ or 6 would clearly be sub-optimal.

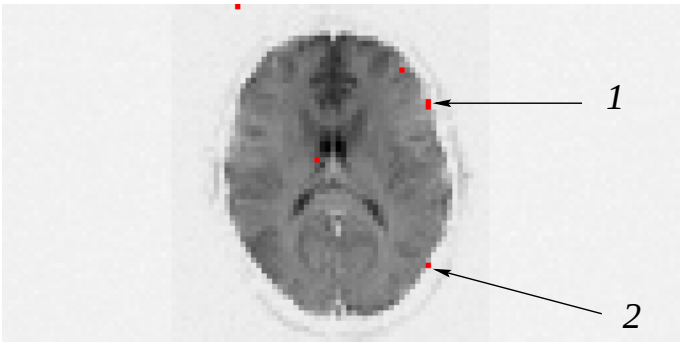

Figure 9. Activation map, superimposed on the raw image

Scale of the drift J	P-value Left inferior frontal lobe (1)	P-value Left posterior temporal lobe (2)
No drift	0.000004	0.000930
7	0.000005	0.000865
6	0.000005	0.000956
5	0.000001	0.000489
4	1.8719e-07	0.000556

Table 1. P-value at two regions of the brain as a function of the scale of the trend.

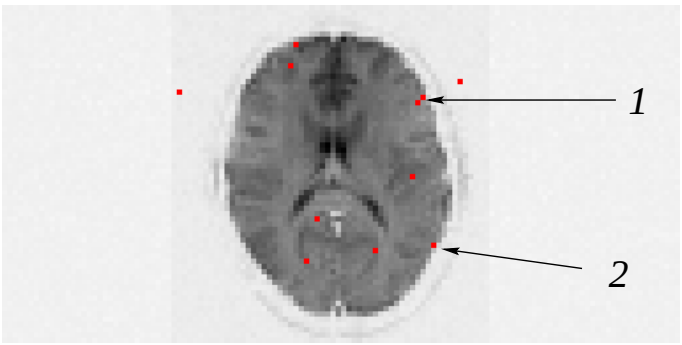

Figure 10. Activation map, superimposed on the raw image

Scale of the drift J	P-value Left inferior frontal lobe (1)	P-value Left posterior temporal lobe (2)
No drift	0.005031	0.036369
7	0.000523	0.002171
6	0.000420	0.000160
5	0.000203	0.000138
4	0.000109	0.000269

Table 2. P-value at two regions of the brain as a function of the scale of the trend.

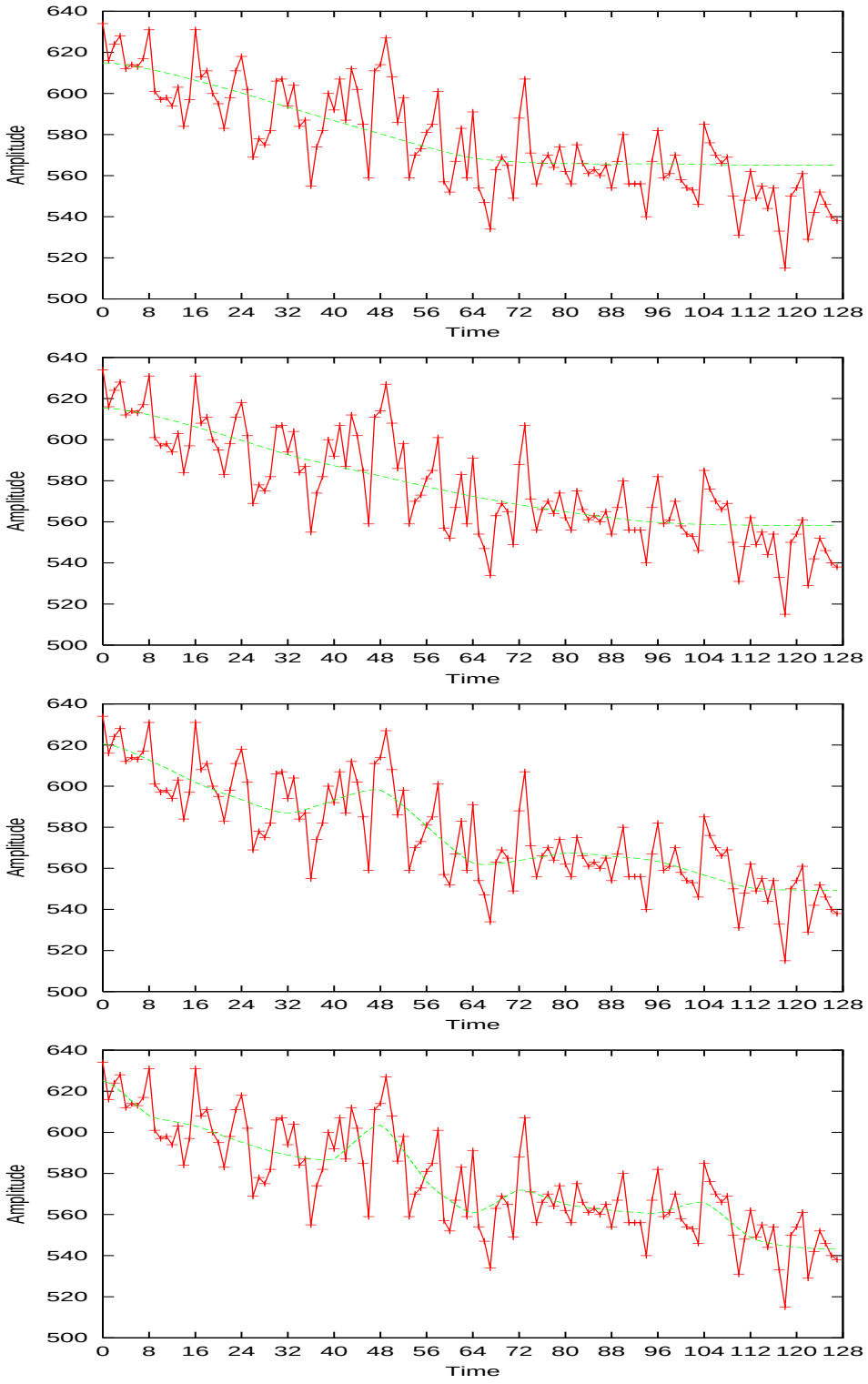

Figure 11. Estimation of the trend for different values of the scale of the trend J. Upper left : $J = 7$, upper right $J = 6$, lower left $J + 5$, lower right $J = 4$.

Acknowledgements

The author thanks Gregory McCarthy, Director of the Brain Imaging and Analysis Center, Duke University, for making the fMRI data available for this work.

REFERENCES

1. I. Vanzetta and A. Grinvald, "Increased cortical oxidative metabolism due to sensory stimulation: implications for functional brain imaging," *Science* **286**, pp. 1555–8, Nov. 1999.
2. P. Jezzard, "Physiological noise: strategies for correction," in *Functional MRI*, C. Moonen and P. Bandettini, eds., pp. 173–182, Springer-Verlag, 1999.
3. M. Lowe and D. Russell, "Treatment of baseline drifts in fMRI time series analysis," *Journal of Computer Assisted Tomography* **23(3)**, pp. 463–473, 1999.
4. G. Glover, "Deconvolution of impulse response in event-related bold fMRI," *NeuroImage* (9), pp. 416–429, 1999.
5. B.B.Biswal, E. DeYoe, and J. Hyde, "Reduction of physiological fluctuations in fMRI using digital filters," *Magnetic Resonance in Medicine* **35**, pp. 107–113, 1996.
6. P. Bandettini, "The temporal resolution of functional MRI," in *Functional MRI*, C. Moonen and P. Bandettini, eds., pp. 205–220, Springer-Verlag, 1999.
7. N. Lange and S. Zeger, "Non-linear Fourier time series analysis for human brain mapping by functional magnetic resonance imaging," *Appl. Statist.* **46**(1), pp. 1–29, 1997.
8. N. Crellin, T. Hastie, and I. Johnstone, "Statistical models for image sequences," Tech. Rep. 205, Department of Statistics, Stanford University, July 1999.
9. A. Vazquez and D. Noll, "Nonlinear aspects of the BOLD response in functional MRI," *Human Brain Mapping* **7**, pp. 108–118, 1998.
10. S. Lai and M. Fang, "A novel local PCA-based method for detecting activation signals in fMRI," *Magnetic Resonance Imaging* **17**, pp. 827–836, 1999.
11. M. Gabbay, C. Brennan, E. Kaplan, and L. Sirovich, "A principal components-based method for the detection of neuronal activity maps: application to optical imaging," *NeuroImage* (11), pp. 313–325, 2000.
12. A. Hyvärinen, "Survey on independent component analysis," *Neural Computing Surveys* , pp. 94–128, 1999.
13. B.B.Biswal and J. Ulmer, "Blind source separation of multiple signal sources of fMRI data sets using independent component analysis," *Journal of Computer Assisted Tomography* **23(3)**, pp. 265–271, 1999.
14. M. McKeown, "Detection of consistently task-related activations in fMRI data with hybrid independent component analysis," *NeuroImage* (11), pp. 24–35, 2000.
15. A. Hyvärinen, "Beyond independent components," in *Proc. Int. Conf on Artificial Neural Networks, Edinburgh, UK*, pp. 809–814, 1999.
16. G. McCarthy, A. Puce, M. Luby, A. Belger, and T. Allison, "Magnetic resonance imaging studies of functional brain activation: analysis and interpretation," *Electroencephalography & Clinical Neurophysiology - Supplement* **47**, pp. 15–31, 1996.
17. B. Vidakovic, *Statistical Modeling by Wavelets*, John Wiley & Sons, 1999.
18. I. T., T. S., and M. Y., "A new segmentation method of electroencephalograms by use of Akaike's information criterion," *Brain Research. Cognitive Brain Research* **3(1)**, pp. 33–40, 1995.
19. P. Durka and K. Blinowska, "In pursuits of time-frequency representation of brain signals," in *Time Frequency and Wavelets in Biomedical Signal Processing*, M. Akay, ed., pp. 389–406, IEEE Press, 1998.
20. F. Meyer, "Multi-components analysis of fMRI," tech. rep., Dept of Electrical Engineering, University of Colorado, 2000.
21. H. Krim, D. Tucker, S. Mallat, and D. Donoho, "On denoising and best signal representation," *IEEE Trans. on Information Theory* **45**, pp. 2225–2238, November 1999.
22. G. McCarthy, M. Luby, J. Gore, and P. Goldman-Rakic, "Infrequent events transiently activate human prefrontal and parietal cortex as measured by functional MRI," *Journal of Neurophysiology* **77**(3), pp. 1630–4, 1997.
23. M. Schlosser, N. Aoyagi, R. Fullbright, J. Gore, and G. McCarthy, "Functional MRI studies of auditory comprehension," *Human Brain Mapping* **6**, pp. 1–13, 1998.